# Supplementary Information

# Engineering Electronic Structures of $Nb_6I_x$ Superatomic Clusters by Metal Atom Incorporation: A First-Principles Study

Dolan Acharya[†], Soumyadeep Bhattacharyya[†], Renna Shakir[‡], and J. Karthikeyan[*,†]

[†]Department of Physics, National Institute of Technology, Durgapur, West Bengal, 713209, India

[‡]Department of Sciences & Humanities, Rajiv Gandhi Institute of Petroleum Technology, Jais, Amethi, Uttar Pradesh, 229304, India

**E-mail:** kjeyakumar.phy@nitdgp.ac.in

## 1 Total Pages: 11

## 2 Total Figures: 9

## 3 Total Tables: 7

## Measurement of HOMO-LUMO gap

**Table T1 HOMO-LUMO gap for pristine $Nb_6I_x$ clusters and centre site of the $MNb_6I_{17}$ clusters using with PBE and HSE06 functionals.**

| Clusters | PBE (eV) | HSE06 (eV) |
|---|---|---|
| $Nb_6I_{12}$ | 0.55 | 1.38 |
| $Nb_6I_{13}$ | 0.18 | 0.73 |
| $Nb_6I_{14}$ | 0.80 | 1.33 |
| $Nb_6I_{15}$ | 0.08 | 0.65 |
| $Nb_6I_{16}$ | 0.07 | 0.50 |
| $Nb_6I_{17}$ | 0.01 | 0.80 |
| $Nb_6I_{18}$ | 0.00 | 0.90 |
| $ScNb_6I_{17}$ | 0.30 | 1.11 |
| $TiNb_6I_{17}$ | 0.31 | 1.26 |
| $VNb_6I_{17}$ | 0.18 | 1.20 |
| $CrNb_6I_{17}$ | 0.19 | 1.33 |
| $MnNb_6I_{17}$ | 0.02 | 1.51 |
| $FeNb_6I_{17}$ | 0.06 | 1.52 |
| $CoNb_6I_{17}$ | 0.24 | 1.10 |
| $NiNb_6I_{17}$ | 0.13 | 0.74 |
| $CuNb_6I_{17}$ | 0.67 | 1.47 |
| $ZnNb_6I_{17}$ | 0.16 | 1.12 |

For pristine $Nb_6I_{18}$ cluster the HOMO-LUMO gap is about to 0.0004 eV for GGA-PBE functional due to the degeneracy of the orbitals as presented in Table T1.

## Force generated by HSE06

The force generated by HSE06 in x, y ,and z direction for different clusters $MNb_6I_{18}$ is shown in Table T2.

**Table T2 Force generated by HSE06 for different clusters**

| Clusters | $F_x$ | $F_y$ | $F_z$ |
|---|---|---|---|
| $VNb_6I_{18}$ | 0.12 | 0.12 | 0.12 |
| $CrNb_6I_{18}$ | 0.11 | 0.11 | 0.11 |
| $MnNb_6I_{18}$ | 0.09 | 0.07 | 0.08 |
| $FeNb_6I_{18}$ | 0.12 | 0.10 | 0.11 |
| $CoNb_6I_{18}$ | 0.15 | 0.15 | 0.14 |
| $NiNb_6I_{18}$ | 0.15 | 0.13 | 0.13 |
| $CuNb_6I_{18}$ | 0.15 | 0.13 | 0.13 |
| $ZnNb_6I_{18}$ | 0.14 | 0.14 | 0.14 |

## Calculation of band-center

The band centre can be obtained using Eq. E1.

$$\text{band center} = \frac{\int_{-\infty}^{E_f} \rho(E)\, dE}{\int_{-\infty}^{E_f} \rho\, dE} \tag{E1}$$

where, $\rho$(E) is the density of the orbitals, and $E_f$ is the Fermi energy level of the states.

## Measurement of average Nb-Nb bond distance ($d_{Nb-Nb}$)

The measurement of average Nb-Nb bond distance ($d_{Nb-Nb}$) for $Nb_6I_x$ pristine clusters are given in Table T3. The average Nb-Nb distance ($d_{Nb-Nb}$) vs. number of Iodine atom (x) is shown in Figure S1.

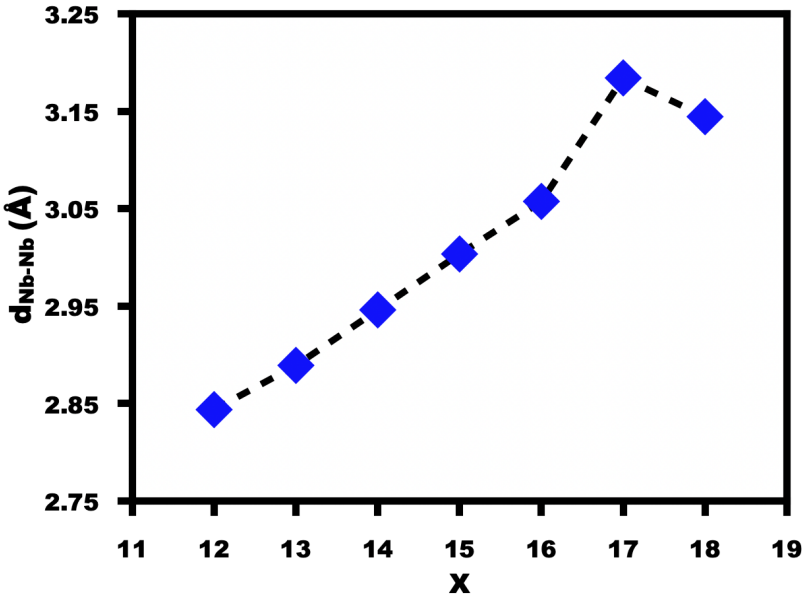


**Figure S1** The average Nb-Nb distance ($d_{Nb-Nb}$) vs. x in pristine clusters.

**Table T3 Average Nb-Nb bond distance for $Nb_6I_x$ pristine cluster**

| $Nb_6I_x$ | $d_{Nb-Nb}$ (Å) |
|---|---|
| $Nb_6I_{12}$ | 2.84 |
| $Nb_6I_{13}$ | 2.89 |
| $Nb_6I_{14}$ | 2.95 |
| $Nb_6I_{15}$ | 3.00 |
| $Nb_6I_{16}$ | 3.06 |
| $Nb_6I_{17}$ | 3.18 |
| $Nb_6I_{18}$ | 3.14 |

## The energy level and their HOMO LUMO gap for pristine $Nb_6I_x$

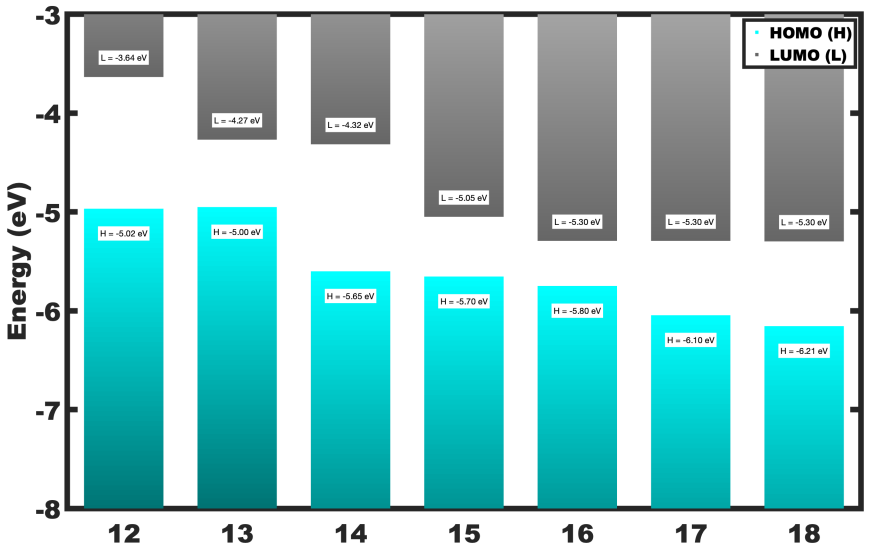


**Figure S2** The energy level in eV of $Nb_6I_x$ using HSE06 functional, where HOMO and LUMO are delineated by the shades of cyan and grey, respectively.

When the I atoms are added within $Nb_6I_{12}$, the Nb atoms are buckled outward, which consequently increases the Nb-Nb bond distance. For example, in the optimized structure of $Nb_6I_{13}$, the Nb atom bonded with the corner I atom significantly buckled outward by increasing the lateral Nb-Nb bond distance to 3.03 Å. While the lateral Nb-Nb bond distance on the opposite of the octahedron remains shorter (= 2.89 Å). Due to the outward pulling of Nb atoms by the corner I atom, the octahedral volume ($V_0$) of $Nb_6I_{13}$ is increased to 10.99 $Å^3$ from the 10.40 $Å^3$ of x = 12. Then, we modelled $Nb_6I_{14}$ cluster by adding one more I atom to two possible sites: the corner site of an adjacent basal Nb atom and the corner site of an opposite apical Nb atom. The total energy shows that the cluster with two I atoms at the opposite corners of apical Nb atoms has slightly lower energy than the other configuration. The $Nb_6I_{14}$ cluster also possesses a stretched octahedron with shorter Nb-Nb bonds between the basal Nb atoms and longer Nb-Nb bonds in the lateral direction due to outward pulling of apical Nb atoms in the opposite corners. The $Nb_6I_{14}$ has a zero magnetic moment and HOMO-LUMO gap of 0.78 eV. The average Nb-Nb and Nb-I bond distances are ($d_{Nb-Nb}$)= 2.95 Å and ($d_{Nb-I}$)= 2.88 Å respectively. When x is raised to 15, the $Nb_6I_{15}$ cluster has much more distortion with a squeezed base and a stretched octahedron due to the asymmetric distribution of corner I atoms, and the $V_0$ becomes 12.29 $Å^3$. In the x = 16 cluster, the cluster has a stretched base with an increased $V_0$ of 12.91 $Å^3$. For x = 17 case, the $V_0$ gets a maximum $V_0$ of 14.75 $Å^3$ due to stretching the octahedron by five corner I atoms. Finally in $Nb_6I_{18}$ having all corners capped with I atoms, the $V_0$ of $Nb_6$ octahedron remains very close to that of the x = 17 cluster with a negligible reduction. The HOMO-LUMO gap for pristine $Nb_6I_x$ is shown in Figure S2.

## Calculation of average bond distance

The average bond distances for center site and 3f-site of $MNb_6I_{18}$ cluster is tabulated in Table T4.

**Table T4 Average bond distance for center site and 3f-site of $MNb_6I_{18}$ cluster.**

| Clusters | Center site | | | 3f-site | | |
|---|---|---|---|---|---|---|
| $MNb_6I_{18}$ | $d_{Nb-Nb}$ (Å) | $d_{Nb-M}$ (Å) | $d_{Nb-I}$ (Å) | $d_{Nb-Nb}$ (Å) | $d_{M-I}$ (Å) | $d_{Nb-I}$ (Å) |
| $ScNb_6I_{18}$ | NA | NA | NA | 3.02 | 2.83 | 2.87 |
| $TiNb_6I_{18}$ | 3.67 | 2.60 | 2.82 | 3.15 | 2.64 | 2.86 |
| $VNb_6I_{18}$ | 3.58 | 2.53 | 2.82 | 3.15 | 2.57 | 2.85 |
| $CrNb_6I_{18}$ | 3.52 | 2.49 | 2.82 | 3.30 | 2.52 | 2.84 |
| $MnNb_6I_{18}$ | 3.47 | 2.45 | 2.82 | 3.25 | 2.54 | 2.84 |
| $FeNb_6I_{18}$ | 3.48 | 2.46 | 2.82 | 3.23 | 2.52 | 2.84 |
| $CoNb_6I_{18}$ | 3.51 | 2.49 | 2.81 | 3.29 | 2.52 | 2.84 |
| $NiNb_6I_{18}$ | 3.52 | 2.52 | 2.82 | 3.41 | 2.53 | 2.83 |
| $CuNb_6I_{18}$ | 3.56 | 2.55 | 2.80 | 3.17 | 2.49 | 2.84 |
| $ZnNb_6I_{18}$ | 3.60 | 2.55 | 2.81 | 3.11 | 2.53 | 2.86 |

## Atomic Energy of 3d-block M atoms

The variation of the elemental atomic energy E(M) in eV for all the 3d-block M atoms (Sc-Zn) is shown in Figure S3.

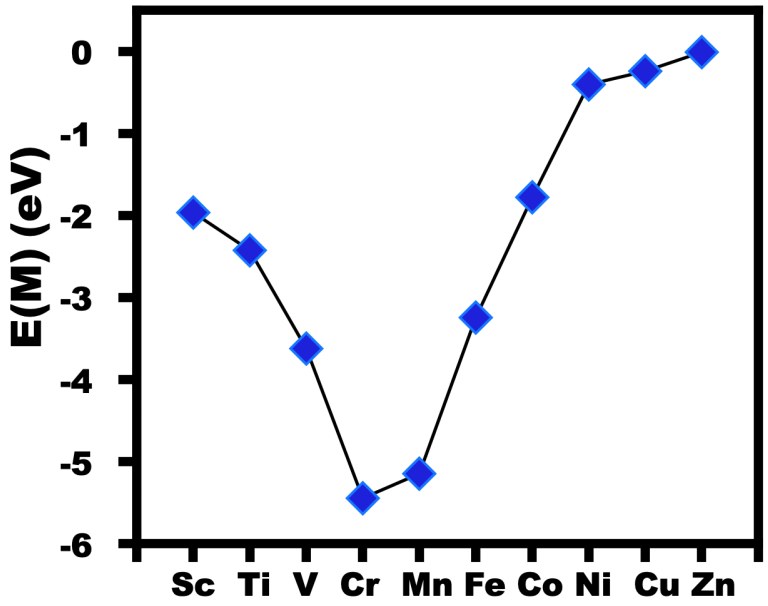


**Figure S3** Atomic energy E(M) in eV for all the 3d-block M(Sc-Zn) atoms.

## Chemical Potential

The variation of chemical potential (eV) of all M atoms

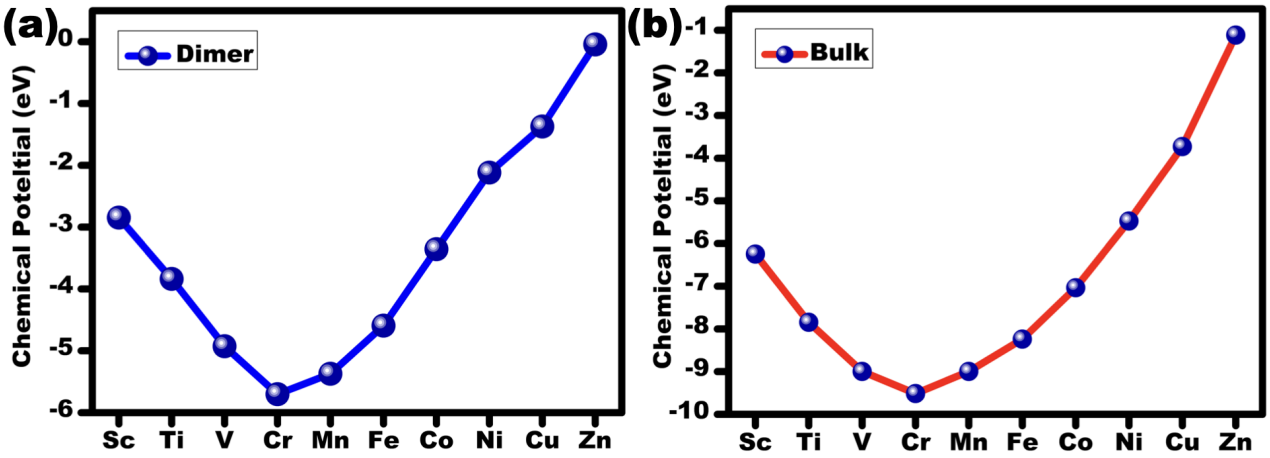


**Figure S4** Chemical potential of different 3d-block M atoms (M=Sc-Zn).

in terms of metal-poor (dimer) and metal-rich (bulk) as shown in Figure S4 (a, b), respectively.

## Molecular Dynamics

The Ab-Initio Molecular Dynamics (AIMD) simulations are performed within the canonical ensemble using a Nosé–Hoover thermostat using a $1\times1\times1$ k-point grid. These simulations are conducted within a temperature range from 700K to 1000K over 3000 femtosecond (fs) time steps. In the total energy plot, the initial 90 steps are omitted due to the starting fluctuations. Furthermore, the vibrational temperature remains constant at around 700 K, as illustrated in Figure S5(a). The initial few steps up to 500 fs have negligible fluctuations during the initial structural vibrations. After 1000 fs, the Co atom crosses the Nb plane to enter the cluster cage as illustrated in Figure S5(b). At T= 700K, the migration of Co from the 3f-site to the center site happens around 1.5 picoseconds (ps). The initial fluctuations become much higher as we elevate the temperature to 1000 K, as shown in Figure S6(a). Similar to the previous phase change, the transition occurs much earlier at approximately 1.3 ps for higher temperatures, as illustrated in Figure S6(b). In the case of the 1000 K simulation, there are a lot more variations in the total energy after the insertion of metal (around 2.2 ps) into the central void due to the distortion in the octahedron. This variation in total energy is not observed in the 700 K simulation. Once the M atom goes inside, it remains confined within the cage and does not escape, even at higher temperatures. The embedded initial and final images in the AIMD simulation clearly illustrate the smooth transition of the Co atom from the initial 3f to the final center site. Thus, our AIMD results distinctly indicate that the Co atom successfully migrates from 3f site into the cage of the $Nb_6I_{18}$ octahedron at elevated temperatures.

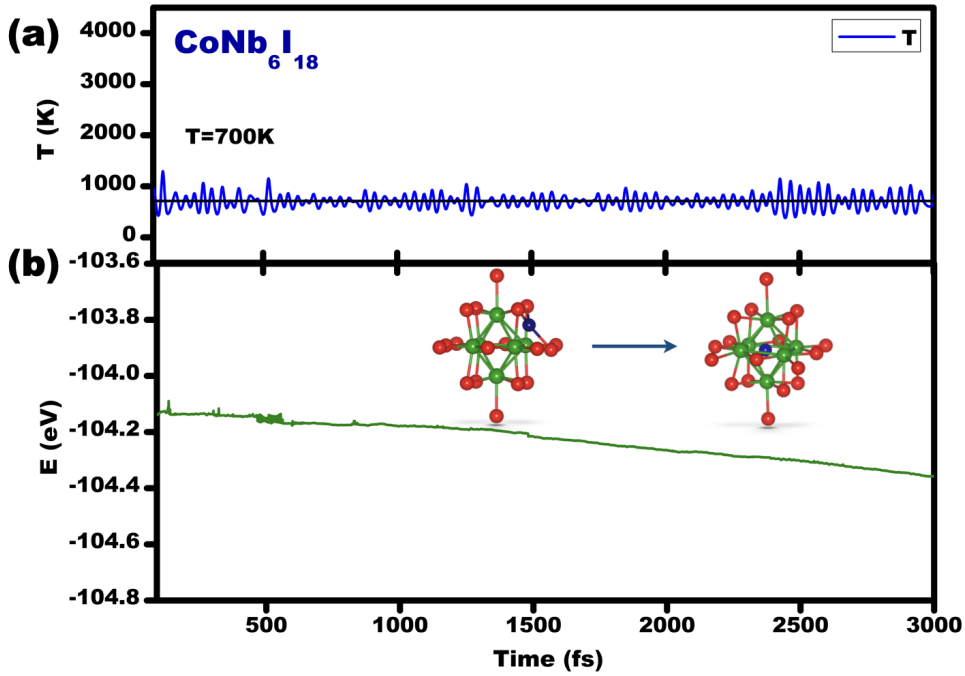


**Figure S5** Molecular dynamics simulation at temperatures 700K for $CoNb_6I_{18}$. In (a) temperature variation over time; and (b) total energy (E) profile with respect to time in femtosecond (fs) indicating structural evolution during the simulation from the 3f site to center site depicting structural stability and transformation.

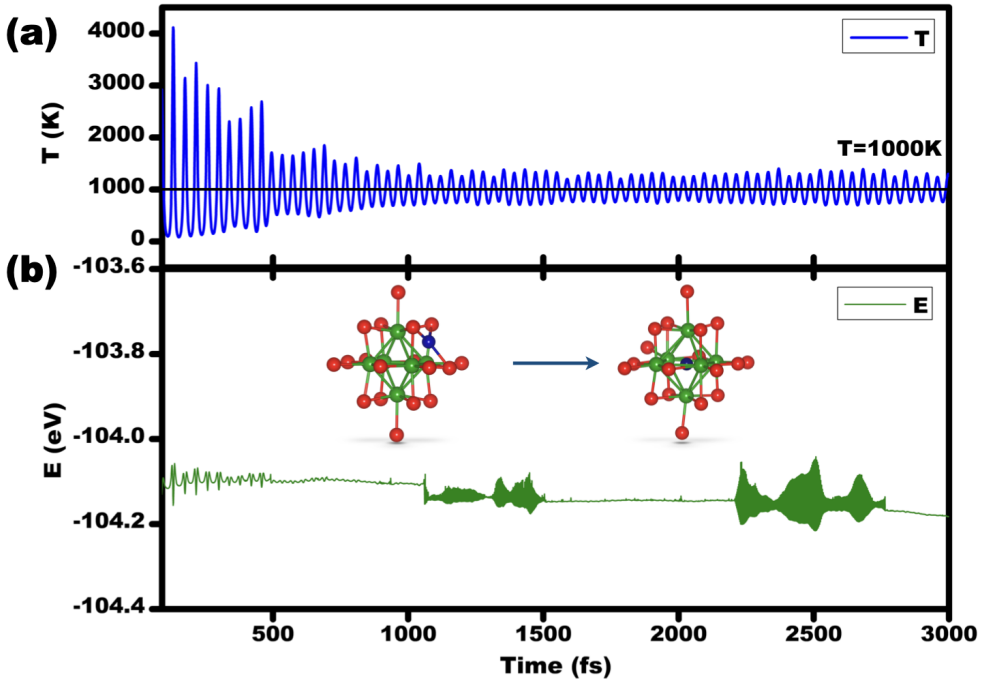


**Figure S6** Molecular dynamics simulation at 1000K for $CoNb_6I_{18}$. In (a) temperature variation over time and (b) total energy (E) profile with respect to time in femtosecond (fs) indicating structural evolution during the simulation from the 3f site to center site depicting structural stability and transformation.

## Measurement of relative energy ($E_R$) for different $I_x$

**Table T5 The $E_R$ difference between the center site and 3f site of $MNb_6I_x$ as given in Table T5.**

| $I_x$ | Clusters | $E_R$ (eV) |
|---|---|---|
| $I_{12}$ | $ScNb_6I_{12}$ | -3.78 |
| | $TiNb_6I_{12}$ | -0.75 |
| | $VNb_6I_{12}$ | -2.07 |
| | $CrNb_6I_{12}$ | -0.66 |
| | $MnNb_6I_{12}$ | -0.56 |
| | $FeNb_6I_{12}$ | -0.52 |
| | $CoNb_6I_{12}$ | -0.43 |
| | $NiNb_6I_{12}$ | -1.91 |
| | $CuNb_6I_{12}$ | -2.90 |
| | $ZnNb_6I_{12}$ | -2.83 |
| $I_{13}$ | $MnNb_6I_{13}$ | -0.26 |
| $I_{14}$ | $CrNb_6I_{14}$ | -1.74 |
| | $MnNb_6I_{14}$ | -0.86 |
| | $FeNb_6I_{14}$ | 0.13 |
| | $CoNb_6I_{14}$ | -0.32 |
| | $CuNb_6I_{14}$ | -1.63 |
| $I_{15}$ | $MnNb_6I_{15}$ | -0.08 |
| | $FeNb_6I_{15}$ | -0.34 |
| | $CoNb_6I_{15}$ | 0.70 |
| | $NiNb_6I_{15}$ | -0.03 |
| | $CuNb_6I_{15}$ | -1.07 |
| | $ZnNb_6I_{15}$ | -0.62 |
| $I_{16}$ | $VNb_6I_{16}$ | -0.01 |
| | $CrNb_6I_{16}$ | 0.74 |
| | $MnNb_6I_{16}$ | 0.28 |
| | $FeNb_6I_{16}$ | 0.01 |
| | $CoNb_6I_{16}$ | 0.56 |
| | $NiNb_6I_{16}$ | 0.44 |
| | $CuNb_6I_{16}$ | -0.65 |
| | $ZnNb_6I_{16}$ | -0.77 |
| $I_{17}$ | $ScNb_6I_{17}$ | -3.96 |
| | $TiNb_6I_{17}$ | -2.28 |
| | $VNb_6I_{17}$ | -0.65 |
| | $CrNb_6I_{17}$ | 0.64 |
| | $MnNb_6I_{17}$ | 1.18 |
| | $FeNb_6I_{17}$ | 1.01 |
| | $CoNb_6I_{17}$ | 1.00 |
| | $NiNb_6I_{17}$ | 0.81 |
| | $CuNb_6I_{17}$ | 0.51 |
| | $ZnNb_6I_{17}$ | 0.39 |

## DOS of Cu and Zn doped $Nb_6I_{18}$

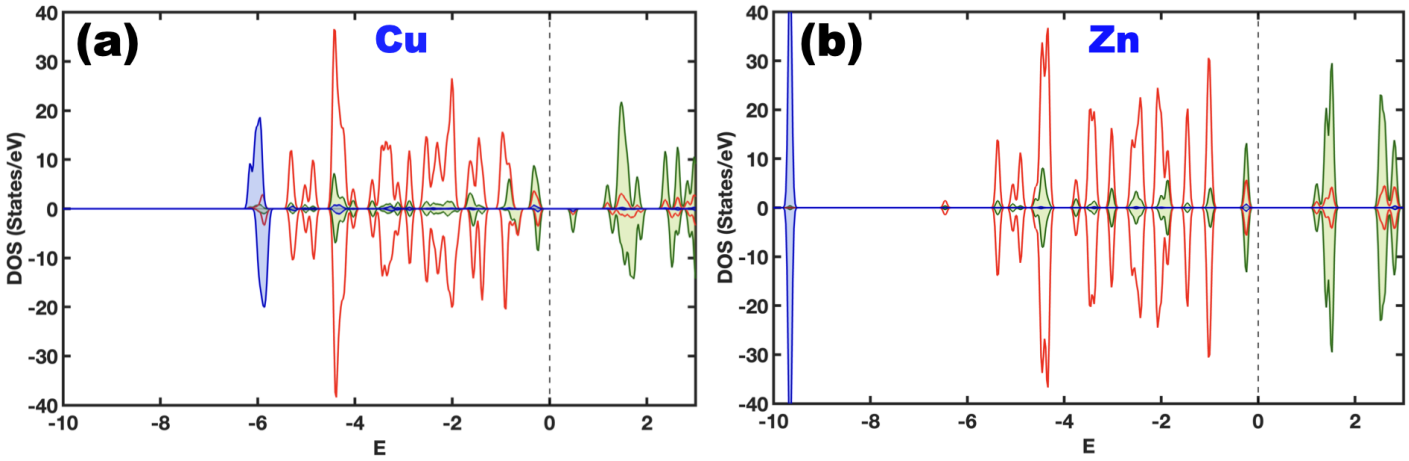


**Figure S7** Density of states (DOS) of $MNb_6I_{18}$, for M = Cu, and Zn

From this DOS plotting, we can clearly see that the M-states for Cu and Zn go much deeper from $E_f$ level as shown in Figure S7.

## The d-band center (DBC) for Nb(4d) and M(3d)

The DBC for these cluster is given in Table T6 using Eq.E1.

**Table T6 The DBC for Nb(4d) and M(3d) calibrates with respect to within vacuum level.**

| Clusters | d-band of Nb(4d) | d-band of M(3d) |
|---|---|---|
| $Nb_6I_{18}$ | -7.93 | NA |
| $VNb_6I_{18}$ | -8.88 | -7.58 |
| $CrNb_6I_{18}$ | -8.70 | -7.52 |
| $MnNb_6I_{18}$ | -8.77 | -8.26 |
| $FeNb_6I_{18}$ | -8.74 | -8.96 |
| $CoNb_6I_{18}$ | -8.63 | -9.15 |
| $NiNb_6I_{18}$ | -8.50 | -9.93 |
| $CuNb_6I_{18}$ | -8.36 | -11.35 |
| $ZnNb_6I_{18}$ | -8.37 | -15.12 |

## HOMO-LUMO gap for $MNb_6I_{18}$

The HOMO, LUMO and their corresponding gap are calibrated with respect to the vacuum of the unit cell by using advanced functional groups like HSE06 to get much better experimentally reliable results. The HOMO LUMO difference is shown in Figure for different functional using GGA+PBE and HSE06. It is prominent that the HOMO LUMO gap is large enough for HSE06 functional, although the trend is almost the same except Fe atom. $CrNb_6I_{18}$ cluster using HSE06 functional in comparison of GGA functional for $ZnNb_6I_{18}$ as shown in Figure S8.

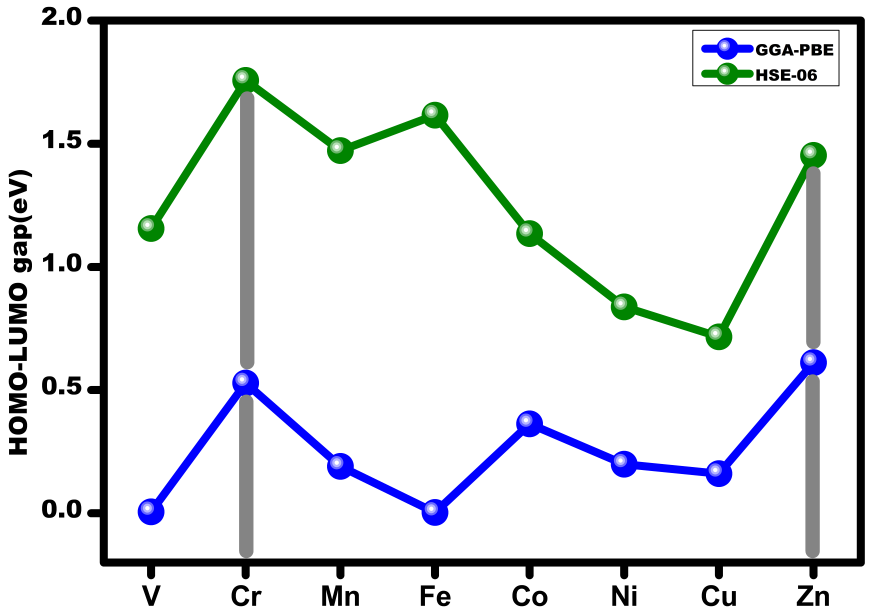


**Figure S8** HOMO-LUMO gap of $MNb_6I_{18}$ using different functional.

## Calculation of Zero Point Energy (ZPE)

The Δ ZPE correction is calculated using the following Eq. E2.

$$\Delta ZPE = \frac{1}{2}\sum_{i=1}^{n} h\nu_i \tag{E2}$$

where, h is the Planck's constant and $\nu$ is the frequency corresponding to the $i^{th}$ vibration. For $H_2$ adsorption, the Δ ZPE is 0.14 eV.

## Calculation of Vibrational Entropy (ΔS)

The vibrational entropy (Δ S) is calculated using the following Eq.s,

$$\Delta S = \sum_{i=1}^{n} S_i \tag{E3}$$

$$S_i = k((x/(e^{-x}-1)) - ln(1-e^{-x})); \tag{E4}$$

$$x = h\nu_i/k_B T \tag{E5}$$

where h is Planck's constant, $k_B$ is the Boltzmann constant, $\nu_i$ is the frequency corresponding to the $i^{th}$ vibration and T denotes the room temperature (298 K).

## Adsorption of second $H_2$ in clusters

The initial protonation readily occurs, with the proton attaching to the Nb plane. The adsorption of a second proton in clusters remains very close to the Nb plane as illustrated in Figure.S9. The interatomic distance between the two H atoms varies from 1.63 to 1.96 , respectively, for all M-doped clusters.

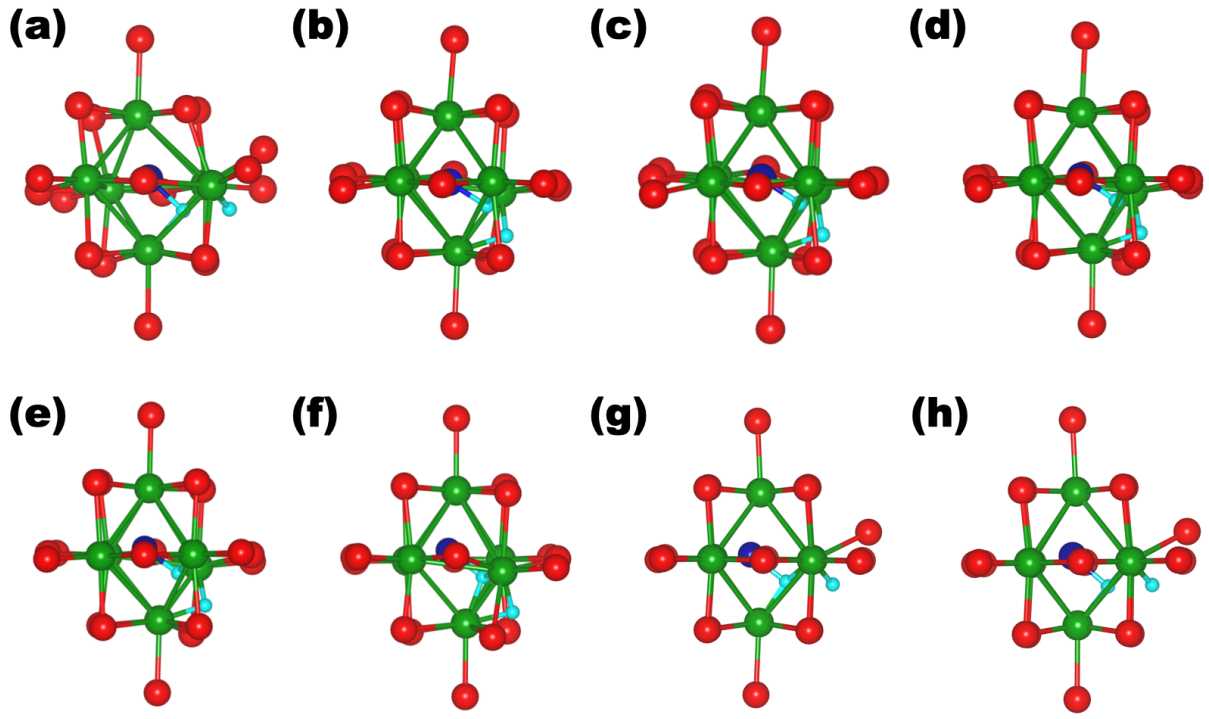


**Figure S9** Adsorption of second $H_2$ in the cluster $MNb_6I_{18}$, M= V to Zn. The green, red, blue and cyan balls represent Nb, I, M and H atoms, respectively.

## Onset potential for HER

The Onset potential of HER is given in Table T7

**Table T7 Onset potential of HER for different clusters**

| $MNb_6I_{18}$ | U-limit (eV) |
|---|---|
| $VNb_6I_{18}$ | 0.50 |
| $CrNb_6I_{18}$ | 0.84 |
| $MnNb_6I_{18}$ | 0.77 |
| $FeNb_6I_{18}$ | 0.59 |
| $CoNb_6I_{18}$ | 0.75 |
| $NiNb_6I_{18}$ | 0.95 |
| $CuNb_6I_{18}$ | 1.19 |
| $ZnNb_6I_{18}$ | 0.87 |
| Pt(111) | 0.66 |